RETRIEVAL< OF BIDIRECTIONAL REFLECTANCE FACTORS AND DIRECTIONAL-HEMISPHERICAI . REFECTANCES USING SPACE-BASED AND AIRBORNE MULTI-ANGLE OBSERVATIONS

John V. Martonchik
Jet Propulsion Laboratory, California Institute of Technology
Pasadena, CA USA 91109

e-mail: john.v.martonchik@jpl.nasa.gov

Abstract -- MISR is scheduled for launch in 1998 on the EOS AM 1 platform. The algorithms needed to analyze data from this instrument are currently being tested, using both simulated data and data currently available from the airborne ASAS multi-angle instrument. The data processing can be divided into three major, sequential *segments*. The first segment retrieves the necessary atmospheric properties over the scene. These results then are used in the second segment to retrieve the surface spectral HDRFs on a pixel-by pixel basis for the scene. Finally, the HDRFs are used with a linearized three parameter BRF model in the third algorithm segment to retrieve the corresponding spectral BRFs. Results of the retrieval algorithms are presented using simulated MISR data.

INTRODUCTION

The Multi-angle imaging SpectroRadiometer (MIS R) is a radiometrically calibrated instrument, scheduled for launch in 1998 on the EOS-AM 1 platform into a sun-synchronous polar orbit. It has nine CCD array cameras, each with a fixed-view angle at the surface, ranging between 70.5° forward and 70.5° aftward, with each camera observing in four spectral bands (443, 555, 670, and 865 run). The spatial sampling of the imagery will be 1.1 km with a swath width of about 360 km. MISR will provide information about aerosol and surface directional reflectance properties on a global basis [1].

The algorithms which are to be used to routinely analyze the multi-angle image data from MISR are currently being tested on simulated MISR data and data from the airborne Advanced Solid-State Array Spectroradiometer (ASAS). These algorithms can be separated into three major segments which are used sequentially. The first segment retrieves the aerosol spectral optical depth and information on the aerosol type [2, 3], which arc needed to characterize *the* radiative properties of the atmosphere over the se-me (for MISR the scene size is a 17.6 km x 17.6 km region). This information then is used as input to the second segment, which retrieves the surface spectral hemispherical-directional reflectance factors (HDRFs) and spectral bihemispherical reflectances (BHRs) [2,4] on a pixel-by pixel basis for the scene, (For MISR the pixel size is 1.1 km x 1.1 km). Finally, the HDRFs arc used in the third algorithm segment to retrieve the corresponding spectral bidirectional reflectance factors (BRFs) and the spectral directional-hemispherical reflectances (DHRs) [4]. This conversion from HDRF to BRF, i.e., removing the effects of direct sunlight, needs to be facilitated with the use of a BRF model since the multi-angle data will have a very limited range of solar zenith angles. The BRF model used is a linearized, three parameter model which is currently being tested on both field and simulated reflectance measurements.

This paper assumes that the atmospheric properties arc known (i e., they have been retrieved from the multi-angle image data using the first segment of the algorithm) and places the emphasis on the surface reflectance retrieval algorithm segments. Results arc presented for simulated MISR data.

THEORY

The top-of-atmosphere (TOA) radiance L_λ at wavelength λ can be written as

$$L_\lambda(-\mu, \mu_0, \phi - \phi_0) = L_\lambda^{atm}(-\mu, \mu_0, \phi - \phi_0) + \exp(-\tau_\lambda/\mu)\, L_\lambda^{surf}(-\mu, \mu_0, \phi - \phi_0) + \int_0^{2\pi}\int_0^1 T_\lambda(-\mu, -\mu', \phi - \phi')\, L_\lambda^{surf}(-\mu', \mu_0, \phi' - \phi_0)\, d\mu'\, d\phi' \quad (1)$$

where μ and μ_0 are the cosines of the view and Sun zenith angles and $\phi - \phi_0$ is the view azimuthal angle with respect to the Sun position. The convention $-\mu$ and μ is used for upwelling and downwelling radiation, respectively. On the right-hnnd-side of Equation (1) L_λ^{atm} is the radiance field scattered by the atmosphere to space without interacting with the surface (i.e., the path radiance), τ_λ is the optical depth of the atmosphere, L_λ^{surf} is the surface-leaving radiance, and T_λ is the upward diffuse transmittance. Equation(1) describes the relationship between thc TOA radiance L_λ and the surface-leaving radiance L_λ^{surf}.

HDRF and BHR Retrieval.

Assuming the atmospheric parameters in Equation (1) are known, L_λ^{surf} can be easily determined by means of an iteration procedure, as described below. Once L_λ^{surf} is determined the HDRF, r_λ, then can be expressed as

$$r_\lambda(-\mu, \mu_0, \phi - \phi_0) = \frac{L_\lambda^{surf}(-\mu, \mu_0, \phi - \phi_0)}{E_\lambda(\mu_0)/\pi} \quad (2)$$

where E_λ is the surface irradiance. From the radiant exitance M_λ, defined as

$$M_\lambda \quad (\mathrm{P}(,) \quad \mathrm{H} = \int_0^{12\pi} \int_0^0 L_\lambda^{surf}(-\mu, \mu_0, \phi - \phi_0)\, \mu\, d\mu\, d\phi \quad (3)$$

the BHR, A_λ^{hem}, is given by the ratio

$$A_\lambda^{hem}(\mu_0) = \frac{M_\lambda(\mu_0)}{E_\lambda(\mu_0)} \cong \frac{M_\lambda(\mu_0)}{E_\lambda^{black}(\mu_0) + s_\lambda \cdot M_\lambda(\mu_0)} \quad (4)$$

where s_λ is the bottom-of-atmosphere bihemispherical reflectance and E_λ^{black} is the black surface irradiance (independent of surface reflection properties). It is related to the actual surface irradiance E_λ by the highly accurate expression .

$$E_\lambda(\mu_0) \cong \frac{E_\lambda^{black}(\mu_0)}{1 - s_\lambda \cdot A_\lambda^{hem}(\mu_0)} \quad (5)$$

Au excellent initial guess for L_λ^{surf} in the iteration procedure can be obtained from Equation (1) by removing L_λ^{surf} from the integral. Thus,

$$L_\lambda^{surf(0)}(-\mu, \mu_0, \phi - \phi_0) = \frac{L_\lambda(-\mu, \mu_0, \phi - \phi_0) - L_\lambda^{atm}(-\mu, \mu_0, \phi - \phi_0)}{\mathrm{Cxp}(-\tau_\lambda/\mu) + t(-p)} \quad (6)$$

where

$$t(-\mu) = \int_0^{12rt} \int_0^0 T_\lambda(-\mu, -\mu', \phi - \phi')\, d\mu'\, d\phi' \quad (7)$$

An initial guess for the 11111{ from Equation (4) implies a guess for M_λ, which can be obtained from Equation (3). The integral in Equation (3) is best easily done by assuming that the surface radiance L_λ^{surf} can be expressed as a two term cosine series in $\phi - \phi_0$,,

$$L_\lambda^{surf}(-\mu, \mu_0, \phi - \phi_0) = L_{0,\lambda}^{surf}(-\mu, \mu_0) + L_{1,\lambda}^{surf}(-\mu, \mu_0) \cdot \cos(\phi - \phi_0) \quad (8)$$

Thus,

$$M_\lambda^{(0)}(\mu_0) = \int_0^1 I_{0,\lambda}^{surf(0)}(-\mu, \mu_0)\, \mu\, d\mu \quad (9)$$

where, for any iteration (n) and using Equation (8)

$$I_{0,\lambda}^{surf(n)}(-P, \mu_0) = \frac{L_\lambda^{surf(n)}(-p, p_o, \phi_a - \phi_0)\cos(\phi_f - \phi_0)}{\cos(\phi_f - \phi_0) \cdot \cos(\phi_a - 4'.)} - \frac{L_\lambda^{surf(n)}(-\mu, \mu_0, \phi_f - \phi_0)\cos(\phi_a - \phi_0)}{\cos(\phi_f - \phi_0) \cdot \cos(\phi_a - \phi_0)} \quad (10a)$$

$$I_{1,\lambda}^{surf(n)}(-\mathrm{P}, \mu_0) = \frac{L_\lambda^{surf(n)}(-\mu, \mu_0, \phi_f - \phi_0)}{\cos(\phi_f - \phi_0) - \cos(\phi_a - \phi_0)} \cdot \frac{L_\lambda^{surf(n)}(-\mu, \mu_0, \phi_a - \phi_0)}{\cos(\phi_f - \phi_0) - \cos(\phi_a - \phi_0)} \quad (10b)$$

Here, ϕ_a and ϕ_f are the two azimuth angles for each fore-aft MISR camera pair.

Once $I_\lambda^{surf(o)}$ is computed, the surface radiance L_λ^{surf} can be updated via the iteration scheme, using Equation (1),

$$\exp(-\tau_\lambda/\mu) \cdot I_\lambda^{surf(n+1)}(-\mu, \mu_0, \phi - \phi_0) = I_\lambda(\mu, \mu_0, \phi - \phi_0) - I_\lambda^{atm}(-\mu, \mu_0, \phi - \phi_0) - \int_0^1 T_{0,\lambda}(-\mu, -\mu')\, L_{0,\lambda}^{surf(n)}(-\mu', \mu_0)\, d\mu' - \cos(\phi - \phi_0) \cdot \int_0^1 T_{1,\lambda}(-\mu, -\mu')\, L_{1,\lambda}^{surf(n)}(-\mu', \mu_0)\, d\mu' \quad (11)$$

The upward diffuse transmittance T_λ in 1 Equation (11) is expressed as a two term cosine series in $\phi - \phi_0$, such that

$$T_{0,\lambda}(-\mu, -\mu') = \int_0^{2\pi} T_\lambda(-\mu, -\mu', \phi')\, d\phi'$$

$$T_{1,\lambda}(-\mu, -\mu') = \int_0^{2\pi} T_\lambda(-\mu, -\mu', \phi - \phi') \cos(\phi - \phi')\, d\phi' \quad (12a, b)$$

Once L_λ^{surf} is updated, it then is used to compute a new M_λ and a new A_λ^{hem}. The iteration proceeds until convergence is reached. This is normally evaluated by noting the change in A_λ^{hem}.

BRF and DHR Retrieval.

The BRF, R_λ, is related to the 1 HDRF, r_λ, through the expression

$$E_\lambda(\mu_0) = r_\lambda(-\mu, \mu_0, \phi - \phi_0) \quad (13)$$

$$= \int_0^{1271} \int_0^{2\pi} R_\lambda(-\mu, \mu', \phi - \phi') L_\lambda^{inc}(P', \mu_0, \phi' - \phi_0) \mu' d\mu' d\phi'$$

where L_λ^{inc} is the radiance incident on the surface. Separating L_λ^{inc} into direct and diffuse components, Equation (13) can be rewritten as

$$E_\lambda(\mu_0) \cdot r_\lambda(-\mu, \mu_0, \phi - \phi_0) = E_\lambda^{dir}(\mu_0) \cdot R_\lambda(-\mu, \mu_0, \phi - \phi_0) \quad (14)$$

$$+ \int_0^{12\pi} \int_0^{11'} R_\lambda(-\mu, 11', \$ - \phi') L_\lambda^{diff}(\mu', \mu_0, \phi' - \phi_0) \mu' d\mu' d\phi'$$

where L_λ^{diff} is the diffuse radiance incident on the surface and E_λ^{dir} is the direct irradiance. They can be expressed as

$$E_\lambda^{dir}(\mu_0) = \mu_0 E_{0,\lambda} \exp(-\tau/\mu_0) \quad (15)$$

$$L_\lambda^{diff}(\mu, \mu_0, \phi - \phi_0) \cong E_{0,\lambda} \cdot T_{0,\lambda}'(\mu, \mu_0) + E_{0,\lambda} \cdot T_{1,\lambda}'(\mu, \mu_0) \cdot \cos(\phi - \phi_0) + \frac{s_\lambda \cdot A_\lambda^{hem}(\mu_0)}{\pi} \cdot E_\lambda(\mu_0) \quad (16)$$

Where $E_{0\lambda}$ is the exo-atmospheric irradiance and $T_{0,\lambda}'$ and $T_{1,\lambda}'$ describe the downward diffuse transmittance in terms of a two term cosine series in $\phi - \phi_0$. Note that the last term in Equation (16) represents approximately the downwelling radiance due to multiple reflections between the atmosphere and the surface. Inserting this expression for L_λ^{diff} in Equation (14) and rearranging terms,

$$R_\lambda^{(n+1)}(-\mu, \mu_0, \phi - \phi_0) = \frac{E_\lambda(\mu_0)}{E_\lambda^{dir}(\mu_0)} \cdot r_\lambda(-\mu, \mu_0, \phi - \phi_0) - \frac{E_{0,\lambda}}{2\pi E_\lambda^{dir}(\mu_0)} \int_0^1 R_{0,\lambda}^{m(n)}(-\mu, \mu') T_{0,\lambda}'(\mu', \mu_0) \mu' d\mu' - \frac{E_{0,\lambda} \cos(\phi - \phi_0)}{2\pi E_\lambda^{dir}(\mu_0)} \int_0^1 R_{1,\lambda}^{m(n)}(-\mu, \mu') T_{1,\lambda}'(\mu', \mu_0) \mu' d\mu' - \frac{s_\lambda \cdot A_\lambda^{hem}(\mu_0) \cdot E_\lambda(\mu_0)}{\pi E_\lambda^{dir}(\mu_0)} \int_0^1 R_{0,\lambda}^{m(n)}(-\mu, \mu') \mu' d\mu' \quad (17$$

Equation (17) is written as an iterative scheme to determine R_λ. Note that R_λ within the integrals is also described by a two term cosine *series in* $\phi - \phi_0$, with coefficients as defined in Equation (12a, b). These coefficients subsequently are replaced by equivalent functions, $R_{0,\lambda}^m$ and $R_{1,\lambda}^m$, generated from a BRF model, because of the lack of measurements concerning the variation of R_λ with p'.

The BRF model used is that of Rahman et al. [5], modified to allow a nearly linearizable least squares fitting analysis. This model has been shown to work sufficiently well for this purpose [6], and is described by,

$$R_\lambda^m(-\mu, \mu_0, \phi - \phi_0) = r_{0,\lambda} \frac{(\mu\mu_0)^{k_\lambda - 1}}{(\mu + \mu_0)^{1 - k_\lambda}} \exp(b_\lambda \cos\Omega) h_\lambda(-\mu, \mu_0, \phi - \phi_0) \quad (18)$$

with three free parameters ($r_{0,\lambda}$, k_λ, b_λ). The function h_λ is a factor to account for the hot spot,

$$h_\lambda(-\mu, \mu_0, \phi - \phi_0) = 1 + \frac{1 - r_{0,\lambda}}{1 + G(-p, \mu_0, \phi - \phi_0)} \quad (19)$$

$$G^2(-p, \mu_0, \phi - \phi_0) = \frac{1 - \mu^2}{\mu^2} + \frac{1 - \mu_0^2}{\mu_0^2} + 2\frac{\sqrt{1 - \mu^2}}{\mu} \frac{\sqrt{1 - \mu_0^2}}{\mu_0} \cos(\phi - \phi_0) \quad (20)$$

and Ω is the scattering angle defined by

$$\cos\Omega = -p\,\mu_0 + \sqrt{1 - \mu^2}\sqrt{1 - \mu_0^2}\cos(\phi - \phi_0) \quad (21)$$

To determine the coefficients $R_{0,\lambda}^m$ and $R_{1,\lambda}^m$ for use in Equation (17), the RPV model R_λ^m in Equation (18) first is fitted to the current iteration of the BRF, $R_\lambda^{(n)}$, to obtain the current iteration of the three model parameters. This fitting is most easily done by comparing the logarithms of R_λ^m and $R_\lambda^{(n)}$ in a least squares sense. Once the three parameters are determined, the BRF model then can be evaluated at all necessary angles in order to compute $R_{0,\lambda}^m$ and $R_{1,\lambda}^m$.

The initial guess for R_λ is set equal to the HDRF, r_λ. Once convergence is achieved for R_λ via Equation (17), the DHR then is evaluated from the expression,

$$A_\lambda^{dir}(\mu_0) = 2\int_0^1 R_{0,\lambda}^{(N)}(-\mu, \mu_0) \mu d\mu \quad (22)$$

where N is the last iteration count and $R_{0,\lambda}^{(N)}$ is computed using the formula displayed in Equation (10a).

EXAMPLES

Application of the retrieval algorithms described in the previous section was accomplished using simulated MISR data. The 1'OA radiances were computed using a multiple scattering, discrete ordinate, radiative transfer code [7] and included both Rayleigh and aerosol scattering. The computations were performed for the MISR red wavelength at 0.670 nm and the nine MISR viewing zenith angles (0°, 5..26.10, ±45.6°, ±60.0°, and ± 70.50), symmetrically placed about the nadir in a single nadir-azimuth angle plane. The solar zenith angle was 55° and the azimuth angle difference between the Sun position and the forward-looking views were set at three values: 30°, 60°and 90° (i.e. perpendicular to tbc principal plane). The aerosol was specified to be a sulfate/ nitrate type (accumulation mode) with phase function asymmetry parameter g = 0.628, single scattering albedo tit = 1.0., and optical depths τ_{aer} of 0.4 and 0.5.

Eleven different surface t ypes, listed in Table 1, were used in tbc MISR TOA radiance calculations. The BRFs for these surfaces were derived from field measurements [8-10] which covered a wide range of both viewing angle and solar zenith angle. These BRFs then were incorporated into the radiative transfer code to simulate a realistic, coupled surface-atmosphere system.

'1'able 1: Surface Type Characteristics

Case	Surface Type	BHR (670nm)
1	Soil	0.186
2	Grassland	0.318
3	Steppe Grass	0.211
4	Hard Wheat	0.228
5	Irrigated Wheat	0.063
6	Hardwood Forest	0.035
7	Pine Forest	0.038
8	Lawn Grass	0.058
9	Corn	0,082
10	Soybean	0.034
11	Orchard Grass	0.077

Example 1: The HDRF was retrieved for each surface type from the simulated multi-angle 1'OA radiances with τ_{aer} =0.4, assuming that the atmospheric properties are ideally known (i.e., no error). Figure 1 shows Lhc retrieval deviation for the eleven surface types and for the three different view-suu azimuth angles. The deviation S is defined as

$$\delta = \frac{1}{9}\sum_{n=1}^{9}\left|r^r(-\mu_n, \mu_0, \phi_n - \phi_0) - r^t(-\mu_n, \mu_0, \phi_n - \phi_0)\right| \quad (23)$$

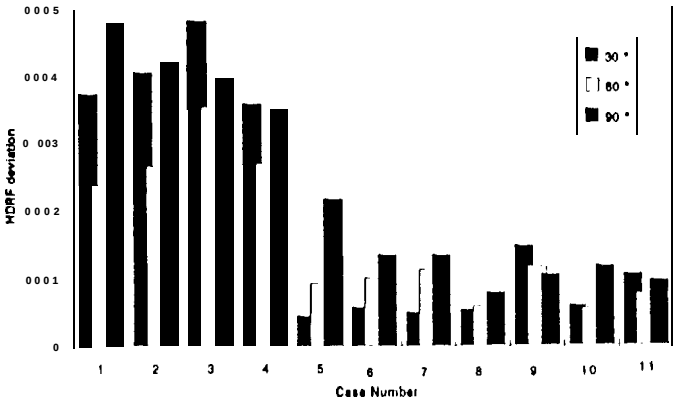

Figure 1, Retrieved 1 II)RF with correct atmosphere.

where r^r and r^t arc tbc retrieved and true BRFs, respectively, at the MISR view angles μ_n, ϕ_n. The absolute accuracy which can be expected from using the retrieval algorithm on MISR data under ideal atmospheric conditions is typically about 2% of the BHR of the surface (note that the BHR for the first four surface types listed in "1'able 1 arc considerably higher that those of the latter seven types), is not strongly dependent on the view azimuth angle, and depends roughly proportionally on the aerosol optical depth.

Example 2: Using the smnc simulated MISR dataset, the 111)RF's were again retrieved, but assuming an aerosol optical depth of 0.35 instead of the true value of 0.4. The results arc shown in Figure 2.

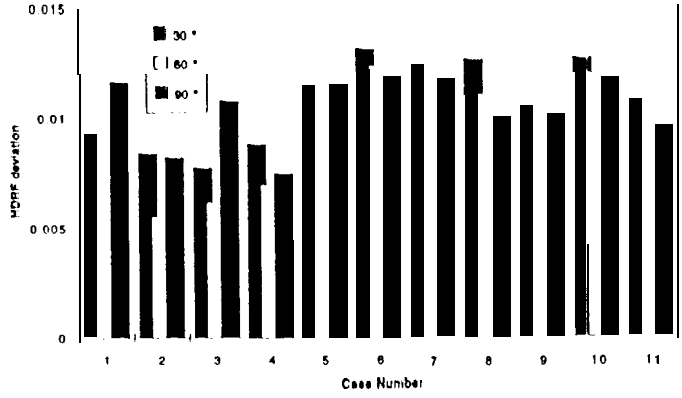

Figure 2. Retrieved I II)RF with incorrect aerosol amount.

This difference of 0.05 is the expected error in retrieved aerosol optical depth using MISR observations. As such, the 1 II)RF deviations shown in Figure 2 arc tbc errors expected from the MISR experiment. No(c that the accuracy for *the* darker surface t ypcs (case number 5 through 11) decreased by about an order of magnitude whereas the brighter surfaces Were somewhat lCSS affected.

Example 3: Using the simulated MISR dataset wi(h τ_{aer} = 0.5 and a Sun-view azimuth angle difference of 30°, Figure 3 shows both HDRF and BRF retrieval results.

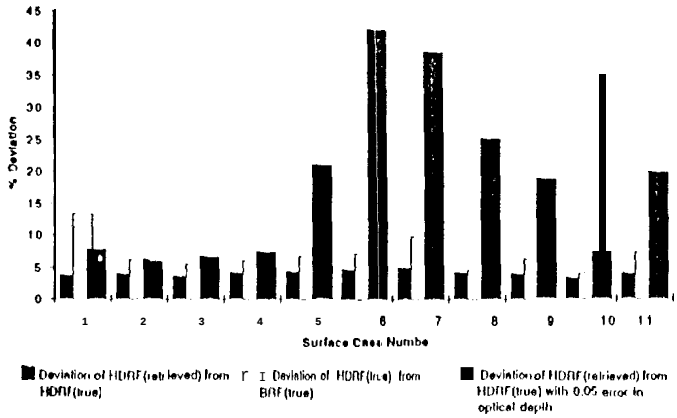

Figure 3. Comparison of HDRF and BRF retrievals.

For each of the eleven surface types, an HDRF retrieval was performed using the correct atmosphere and also one in which the aerosol optical depth was in error by 0.05. Starting from the retrieved HDRFs, obtained using the correct atmosphere, a BRF retrieval was then performed for each case. Figure 3 shows that the expected HDRF errors are generally comparable to or larger than the actual difference between the HDRF and BRF.

SUMMARY

The algorithms to be used by MISR to retrieve the surface HDRF and BRF from radiometrically calibrated multi-angle imagery are currently being tested on simulated MISR data and airborne ASAS data. The results from the simulated MISR data show that the intrinsic accuracy of the HDRF retrieval algorithm is limited mainly by the accuracy of the information on the atmospheric optical properties and not by the limited viewing geometry of the observations. Also, the expected atmospheric properly uncertainties will generally tend to mask any differences in the HDRF and the BRF.

ACKNOWLEDGMENTS

The author would like to express his appreciation to Brian Rheingans for his assistance in the graphical aspects of this work. This research was carried out by the Jet Propulsion Laboratory, California Institute of Technology, under contract with the National Aeronautics and Space Administration.

REFERENCES

[1] Diner, D .J., C.J. Bruegge, T.Deslis, V.G. Ford, L.E. Hovland, D.J. Preston, M .J. Shterenberg, E.B. Villegas, and M.L. White (1993), "1)evelopment status of the EOS Multi-angleImaging StrectroRadiometer (MIS]<)." *SPIE Proc.* 1939,94-103.

[2.] Martonchik, J.V. (1996) " Determination of aerosol optical depth and land surface directional reflectances using multi-angle imagery," submitted for publication in *J. Geophys. Res.*

[3] Diner, D.J., W.A. Abdou, T.P. Ackerman, K. Crean, H.R. Gordon, R.A. Kahn, J.V. Martonchik, S.R. Paradise, M . Wang, R.A. West, J. Zong (1996), "MISR Level 2 Aerosol Retrieval Algorithm Theoretical Basis," *JPL-D11400, Rev. B.*

[4] Diner, D.J., J.V. Martonchik, C. Borel, S.A.W. Gerstl, H.R. Gordon, R. Myneni, B. Pinty, M. Verstraete (1996), "MISR Level 2 Surface Retrieval Algorithm Theoretical Basis," *JPL-D11401, Rev. B*

[5] Rahman, H., B. Pinty, and M.M. Verstraete (1994), "Coupled surface-atmosJ~hcrc reflectance (CSAR) model. Semi-empirical surface model usable with NOAA Advanced Very I ligh Resolution Radiometer data," *J. Geophys. Res.* 98, 20791-20801.

[6] Engelson, 0., B.D. Pinty, M.M. Verstraete, and J.V. Martonchik (1996), "Parametric bidirectional reflectance factor (BRF) models: Evaluation, improvements and applications", Internal report., Space Applications Institute, EC Joint Research Centre, Ispra, Italy.

[7] Grant, I.P. and G.E. Hunt (1968), "Solution of radiative transfer problems using the invariant S_n method," *Mon. Not. Roy. Astron. Soc.,* 141,27-41.

[8] Kimes, D.S. (1983), "Dynamics of directional reflectance factor distributions for vegetative canopies," *Appl. Opt.* 22, 1364-1372.

[9] Kimes, 1). S., W.W. Newcomb, R.F. Nelson and J.B. Schutt (1985), "Directional reflectance distributions of a hardwood and pine forest canopy", *IEEE Trans. Geosci. Remote Sensing* **GE-24**, *281-293.*

[10] Kimes, 1). S., W.W. Newcomb, C.J. Tucker, 1.S. Zonneveld, W. Van Wijngaarden, J. de Leeuw, and G.F. Epema (1985), "Directional reflectance factor distributions for cover types of Northern Africa in NOAA 7/8 AVHRR bands 1 and 2," Remote Sens. Environ. **18**, 1-19.